Article

Chinese Science Bulletin

Geophysics

June 2012 Vol.57 No.16: 1990–1997
doi: 10.1007/s11434-012-5014-5

Static slip model of the M_w 9.0 Tohoku (Japan) earthquake: Results from joint inversion of terrestrial GPS data and seafloor GPS/acoustic data

DIAO FaQi*, XIONG Xiong & ZHENG Yong

State Key Laboratory of Geodesy and Earth's Dyanmics, Institute of Geodesy and Geophysics, Chinese Academy of Sciences, Wuhan 430077, China

Received November 24, 2011; accepted January 19, 2012; published online March 8, 2012

Based on co-seismic displacements recorded by terrestrial GPS stations and seafloor GPS/acoustic stations, the static slip model of the 2011 M_w 9.0 Tohoku earthquake was determined by inverting the data using a layered earth model. According to *a priori* information, the rupture surface was modeled with a geometry that is close to the actual rupture, in which the fault dip angle increases with depth and the fault strike varies with the trend of the trench. As shown by the results inferred from the joint inversion, the "geodetic" moment is 3.68×10^{22} N m, corresponding to M_w 9.01, and the maximum slip is positioned at a depth of 13.5 km with a slip magnitude of 45.8 m. Rupture asperities with slip exceeding 10 m are mainly distributed from 39.6 to 36.97°N, over a length of almost 240 km along the trench. The slip was mostly concentrated at depths shallower than 40 km, up-dip of the hypocenter. "Checkerboard" tests reveal that a joint inversion of multiple datasets can resolve the slip distribution better than an inversion with terrestrial GPS data only—especially when aiming to resolve slip at shallow depths. Thus, the joint inversion results obtained by this work may provide a more reliable slip model than the results of other studies that are only derived from terrestrial GPS data or seismic waveform data.

M_w 9.0 Tohoku earthquake, static slip model, terrestrial GPS data, seafloor GPS/acoustic data, curved rupture surface

Citation: Diao F Q, Xiong X, Zheng Y. Static slip model of the M_w 9.0 Tohoku (Japan) earthquake: Results from joint inversion of terrestrial GPS data and seafloor GPS/acoustic data. Chin Sci Bull, 2012, 57: 1990–1997, doi: 10.1007/s11434-012-5014-5

On 11 March, 2011, the M_w 9.0 Tohoku earthquake occurred on the trench northeast of Japan. This earthquake and the secondary disasters, including tsunami and nuclear leakage, caused massive damage to human life and infrastructure. Both the GCMT and the USGS WPhase results indicate the moment magnitude of this earthquake is up to 9.0, which makes this earthquake one of the largest earthquakes ever recorded by modern instruments. Due to the subduction of the Pacific Plate beneath the North American Plate, many earthquakes of M_w 7.0–8.0 have occurred along the trench off northeastern Japan in the past century (Figure 1). However, there has been no record of an earthquake in the area with a magnitude of 9.0 until this one. In addition, ruptures of historic earthquakes are irregularly distributed along the trench, which means that some regions are ruptured repeatedly, whereas other regions seem locked to fault ruptures. A reliable determination of the slip distribution of this M_w 9.0 earthquake is important for understanding the relationships between this earthquake and historic earthquakes, as well as being meaningful for helping to assessing the regional seismic hazards. However, since this earthquake occurred on the trench, and the rupture zone is under water, it is difficult to obtain information on the ruptures from field investigations. Therefore, the only way available is to invert for the slip distribution based on other kinds of observations, such as geodetic and seismological measurements.

A slip model can now be obtained from a seismic waveform inversion or a geodetic inversion, or joint inversions of multiple kinds of datasets. Several models concerning either

*Corresponding author (email: faqidiao@asch.whigg.ac.cn)

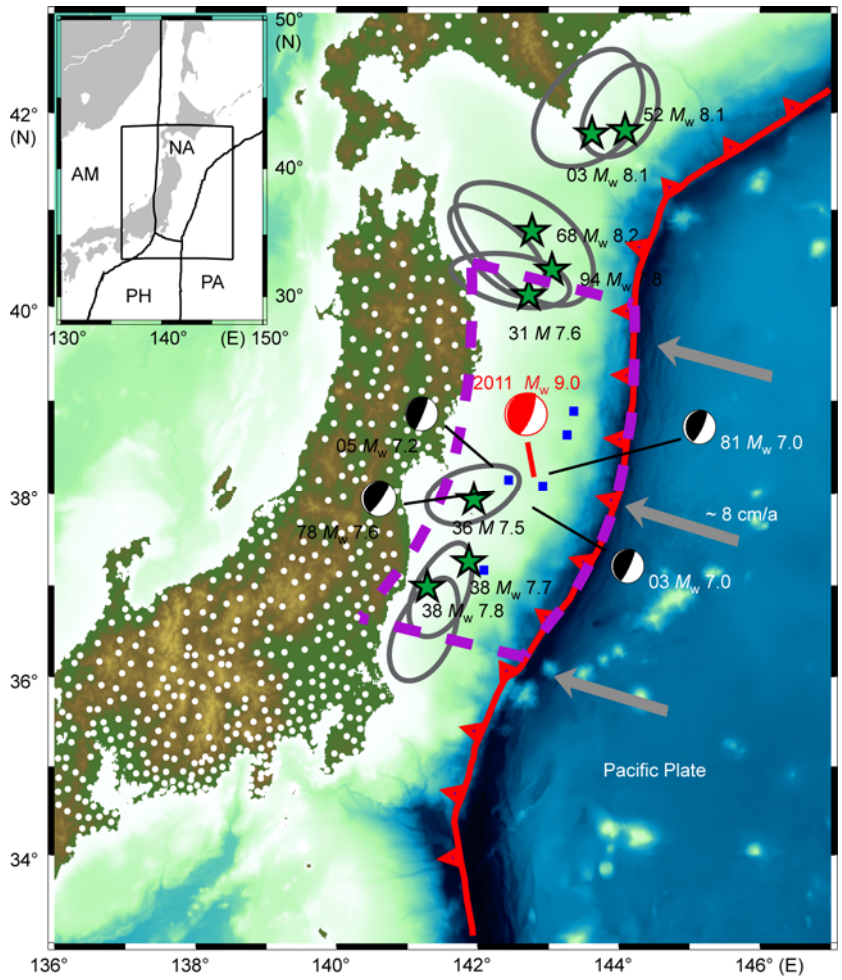

Figure 1 Tectonic setting of the M_w 9.0 Tohoku earthquake. The red beachballs show the focal mechanisms of the main shock (after http://earthquake.usgs.gov/earthquakes/seqs/events/usc0001xgp/). The purple dashed line is the surface projection of the fault rupture plane. The green stars and gray ellipses indicate epicenters and source regions, for large interplate earthquakes ($M_w \geqslant 7.5$) that occurred in the past century, respectively. Four black beachballs show the locations and the focal mechanisms of four earthquakes that occurred close to the epicenter of the main shock. The white dots are GPS stations and the five blue squares illustrate the seafloor GPS/acoustic stations. AM, the Amurian Plate; PH, the Philippine Plate; PA, the Pacific Plate; NA, the North American Plate.

the rupture processes or static slip distributions were published soon after the Tohoku earthquake [1–11]. However, significant discrepancies can be found between these models even though they all inverted moment magnitudes for this quake at around M_w 9.0, and generally obtained slip models that fit their observations as well. For example, inversions from strong motion or seismic waveform data indicate the slip maximum varies between 25 m and 60 m [1–7]. Simons et al. [8] demonstrated that the maximum slip was about 45 m using a joint inversion of terrestrial GPS data and teleseismic waveform data, whereas Hao et al. [9] obtained a maximum slip of 54 m with a similar dataset and inversion method. As for the static slip distribution of the earthquake, the joint inversion model with terrestrial GPS data and tsunami waveform data developed by Simons et al. [8] shows that the maximum static slip reached up to 60 m, whereas the static slip models inferred only from terrestrial GPS data show the slip maximum is only around 25 m [10,11].

Differences in the geometric parameters of the fault and smoothing constraint used in the inversions might be responsible for the discrepancies between the different models. However, another important factor may be even more important. Since almost all of the models mentioned above are based on far-field datasets, such as the seismic waveform data or GPS data that are obtained on the Japanese islands and other regions, no near-field constraint has been considered in their models. Although the GPS stations are densely distributed on the islands, this dataset cannot constrain the fault slip well. This is especially so for asperities located at shallow depths on the rupture surface. Fortunately, above the source region there are five seafloor GPS/acoustic stations, which can provide near-field co-seismic displacement information. Although there are only five stations, the measured seafloor GPS/acoustic co-seismic displacement data can provide significant constraints on the fault slip. For

this reason, we have built a static slip model of the M_w 9.0 Tohoku earthquake based on the joint inversion of the seafloor GPS/acoustic data and terrestrial GPS data.

1 Data

Continuous GPS data provided by the Geospatial Information Authority (GSI) of Japan were processed by the ARIA group at the U.S. Jet Propulsion Laboratory (JPL) using GIPSY software. The standard deviation of the static 3D co-seismic displacements on terrestrial GPS stations is about 3 cm (ftp://sideshow.jpl.nasa.gov/pub/usrs/ARIA, Figure 2, black arrows). These co-seismic displacements were determined by observations 6 min before and 9 min after the main shock. Since the measurement times were very close to the occurrence time of the main shock, the displacements mainly correspond to the co-seismic movement.

Seafloor co-seismic displacements were determined from GPS/acoustic observations before and after the earthquake (Figure 2, red arrows). However, the most recent observations prior to the event were carried out between November 2010 and February 2011, and the next observations after the event were conducted from 28 March to 5 April. So, the resulting seafloor displacement determinations are probably contaminated by deformation induced by foreshock, aftershock and aseismic afterslip. Fortunately, as analyzed by Sato et al. [12], the effects of such factors are negligible compared with the co-seismic faulting. Therefore most of the GPS/acoustic observed seafloor co-seismic displacements are induced by co-seismic rupture.

2 Method

We have conducted a geodetic inversion to estimate the co-seismic slip distribution on a curved fault surface, for which the strikes are generally fixed along the trend of the trench. In addition, based on previous seismic imaging [13], the dip angles of the rupture surface were defined to increase progressively from 6° at the top to 23° at the bottom of the fault. Overall, the geometry of the rupture is consistent with the slab contours of Huang et al. [14], and should be more reasonable than other widely used planar faults.

We fixed the two ends of the fault surface by the distribution of aftershocks that occurred in the initial stage after the main shock. The spatial coverage of the fault surface is shown in Figures 1 and 2, with an area of around 480 km × 240 km. In order to invert for the slip distribution, the fault surface was divided into 288 sub-faults that were each 20 km × 20 km in area. A constrained least squares method was employed to invert for the slip models [15], in which an *a priori* smoothing constraint was added to make the solution stable and reasonable. The following cost function was defined and the steepest descent method was applied to search for the optimal solution.

$$F(b)=\|Gb-y\|^2+\alpha^2\|H\tau\|^2.$$

In the equation, G is the Green's function; y is the observation vector; b is the vector formed by the slip of each sub-fault; H represents the finite difference approximation of the Laplacian operator; α is the smoothing factor, which controls the trade-off between model roughness and data

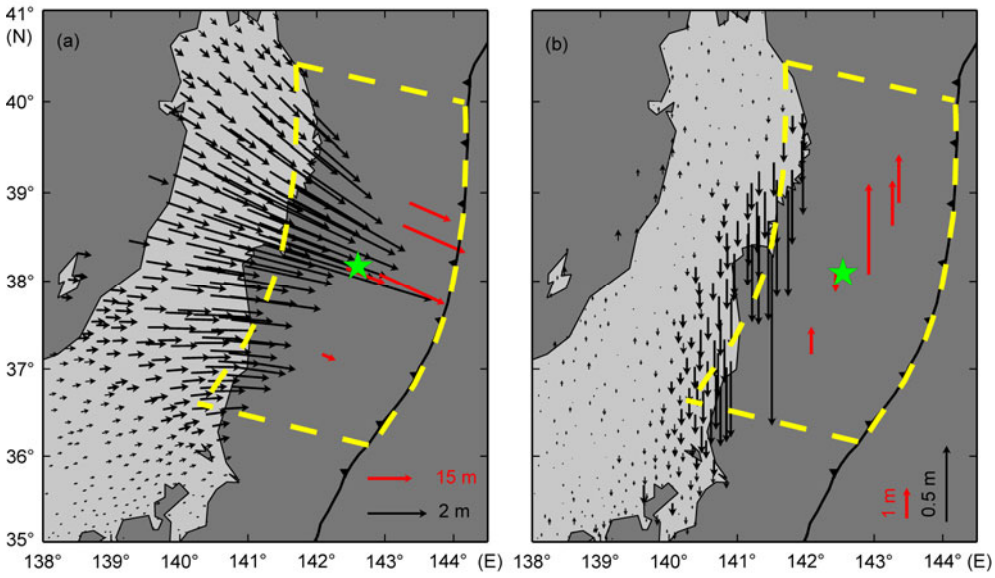

Figure 2 Co-seismic displacements used in the inversion. Black arrows denote the terrestrial GPS observations (http://supersites.earthobservations.org/sendai.phd), while red arrows represent seafloor GPS/acoustic co-seismic displacements. The green star is the epicenter and the dashed line is the projected surface of the curved fault surface.

misfit. A layered earth model derived from CRUST 2.0 [16] was employed to calculate the Green's functions, and the medium parameters on the hanging wall were used as all observations are distributed on the hanging wall. We neglected the effects of lateral heterogeneity and topography in our inversion. Figure 3 shows the trade-off between model roughness and data misfit, from which we chose a reasonable smoothing factor and thus generated the optimal solution. In addition, we also ran the inversion with the same fault geometry and a half-space model to investigate how, and to what extent, crustal layering could affect the slip model.

3 Results and discussion

Figure 4(a) illustrates the slip distribution jointly inverted from the data based on the fault parameters mentioned above.

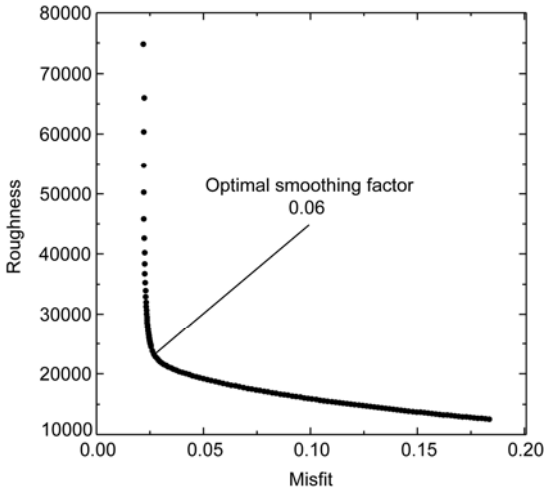

Figure 3 Trade-off curve with data misfit plotted as a function of the model roughness and the stress drop. The misfit is the relative residual and the roughness is the normalized value.

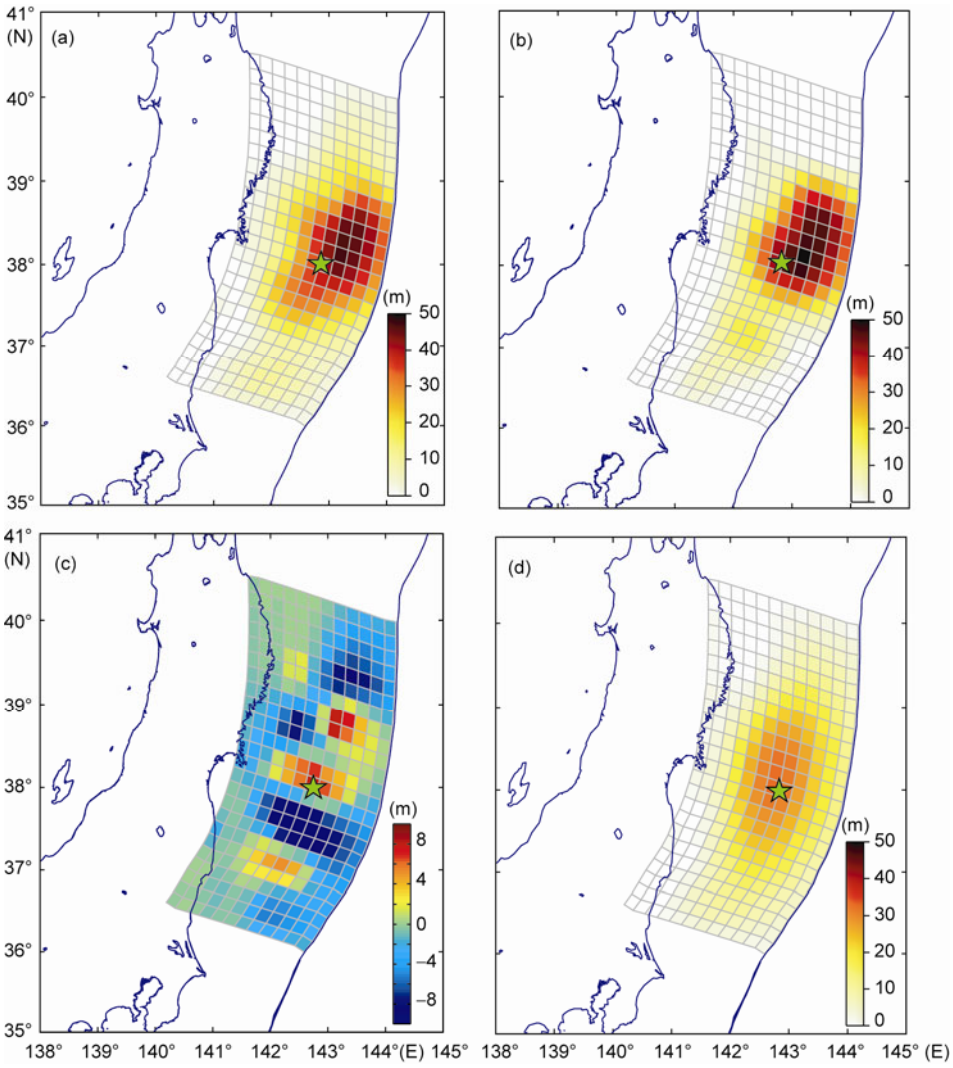

Figure 4 Slip distributions resulting from (a) jointly inverted data with a layered earth structure, and (b) jointly inverted data with a homogeneous half-space structure. (c) is the difference between (a) and (b), and (d) is the slip model inferred from terrestrial GPS data alone with a layered earth structure.

With a "geodetic" moment of 3.68×10^{22} N m (corresponding to M_w 9.01), a slip maximum of 45.8 m was found at (143.2°E, 38.11°N) and a depth of 13.5 km. In addition, the length of the rupture area with a slip >10 m is about 240 km, extending from 39.6 to 36.97°N and mostly located at depths shallower than 40 km. The derived slip concentration is generally consistent with the highly "coupled" area inferred from inter-seismic terrestrial observations [17,18]. However, it seems that the highly coupled area is just deeper than the area of concentrated slip and closer to the coastline of northeastern Japan. This phenomenon is perhaps partially due to the fact that the highly coupled areas were derived from only the onshore inter-seismic ground velocities, which cannot adequately constrain the area of fault coupling far from the coastline. A slightly left-lateral strike slip component was found in our slip model, which shows general agreement with the focal mechanisms of this earthquake and the historic earthquakes from this region, indicating the consistency between our slip model and the tectonic environment.

A comparison of the slip distributions inverted from layered and homogeneous half-space models is shown in Figure 4. The moment of the slip model inferred from the half-space medium is 3.13×10^{22} N m (M_w 8.96) for a given shear modulus of 40 GPa and Poisson's ratio of 0.25. This is 14% less than that inferred from the layered earth model. With a slip maximum of 49.7 m, the slip model derived from the half-space earth structure slightly overestimates slip values in the concentrated slip area while underestimating slips surrounding the concentrated slip area (Figure 4(b) and (c)). The area with fault slip exceeding 10 m is about 170 km long in the half space model, extending from 38.8 to 37.4°N, which is clearly less than that of the slip model inverted from the layered earth model (240 km). This means that slip distribution derived from the half-space model is more compact. The slip model inverted from only the terrestrial GPS data is shown in Figure 4(d). With a moment magnitude of about 8.95, the slip maximum is about 25 m, much less than the slip maximum inferred from the joint inversion of terrestrial GPS and seafloor data. In addition, the slips are mostly located deeper in this model than those from the joint inversion.

Our optimal slip model explains almost all of the observations (>99%), including near-field seafloor GPS/acoustic data and far-field terrestrial data (Figure 5). The RMS errors in three orientations (East, North and Up) are respectively

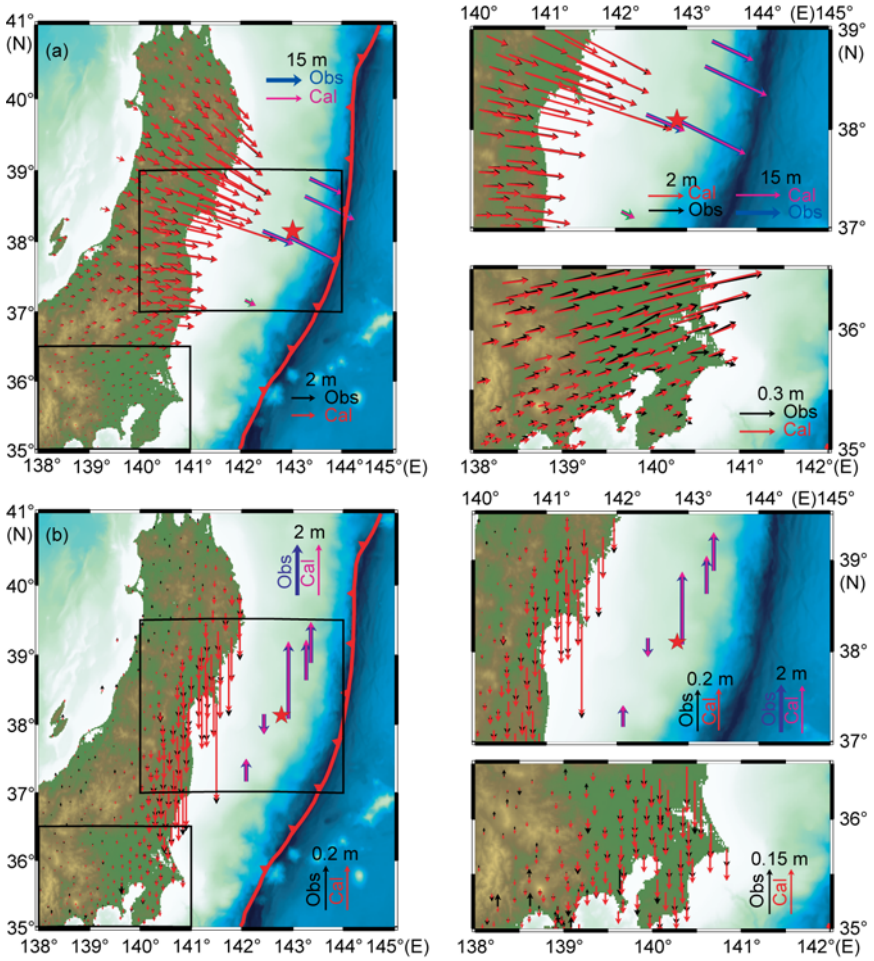

Figure 5 Comparison between observations and predictions from the optimal slip model.

2.1, 2.5 and 3.6 cm for the layered earth model, and 2.7, 4.0 and 2.8 cm for half-space model. The RMS errors for the two earth structures are located at almost the same level. However, the half-space model overestimates the far-field displacements systematically from the residual distribution (Figure 6(b)). This drawback of the half-space model was also found by Pollitz et al. [19]. As the layered earth model is closer to the real earth structure, we argue that the slip distribution derived from the layered model should be more reasonable.

From a "checkerboard" test (Figure 7) we clearly find that the terrestrial GPS data can only resolve the slip at greater depths, while the slip distribution can be well resolved at any depth by incorporating the seafloor data. Checkerboard tests indicate the importance of the near-field data in the slip model inversions. In addition, the weak resolution ability of the terrestrial GPS data is likely because of the long distance from the observation stations to the fault patches

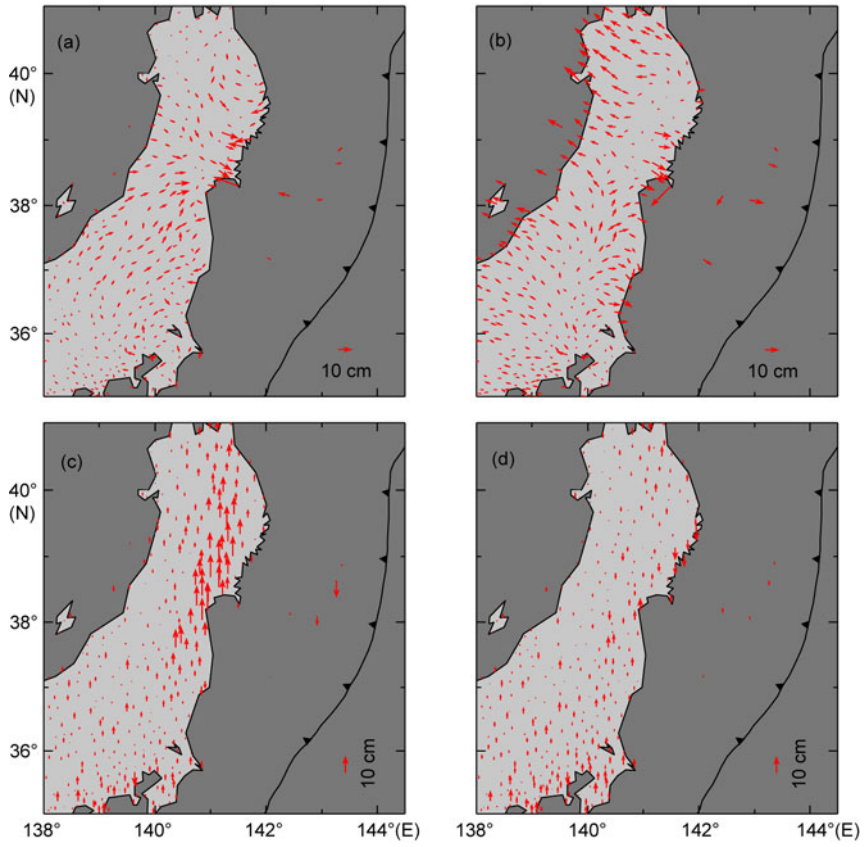

Figure 6 Horizontal and vertical residuals of co-seismic offsets. (a), (c) Residuals in the layered earth model; (b), (d) those in the half-space model.

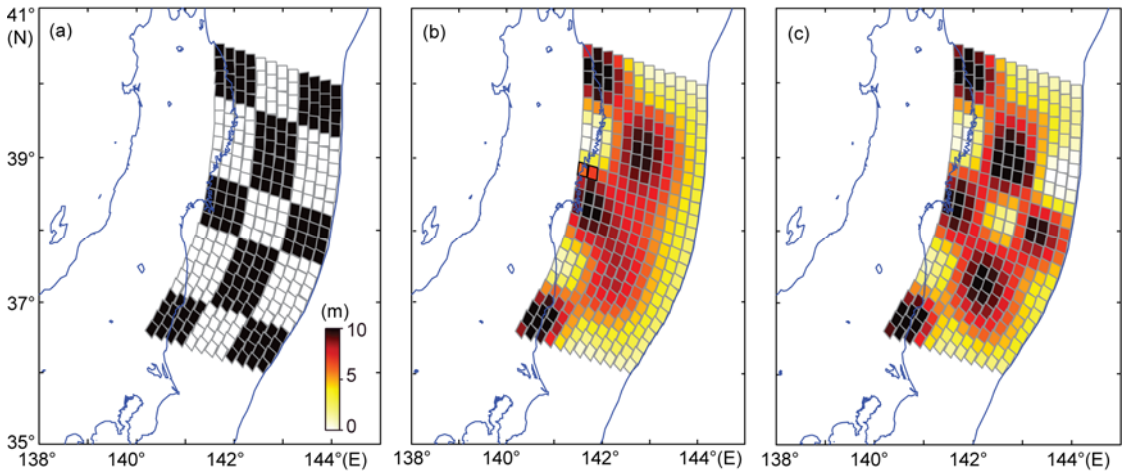

Figure 7 Checkerboard tests with different datasets. Input mode (a), inverted slip distribution using only terrestrial GPS data (b) and joint data (c).

rather than the inversion method itself. With far-field constraints only, the inverted model can only provide a general survey of the slip distribution due to the incompleteness of observations and the non-uniqueness in the inversion. However, if more observational data are introduced into the slip distribution inversion, especially near-field observations, our constraints on the slip behavior should also improve.

Several preceding historical ruptures (~M_w 7.0) occurred in the maximum slip region of this M_w 9.0 event over the preceding 85 years. However, it would appear that these ruptures did not release the accumulated elastic strain in this region, because the M_w 9.0 event ruptured the asperity again only a few decades later. The 2011 rupture cannot be explained by the strain accumulation in the 30 years after the 1981 M_w 7.0 earthquake. This history of strain accumulation indicates that the fault was highly locked and apparently cannot be fully released by repeat ruptures of ~M_w 7.0 earthquakes.

Aftershocks in the three months following the main shock were roughly complementary with the co-seismic slip distribution, i.e. the aftershocks mostly occurred down dip and at the two ends of the area of slip concentration of this earthquake (Figure 8). In addition, afterslips in the initial stage following the main shock mainly occurred at the down-dip extension of the main rupture [10,11]. Aftershocks and afterslips can probably be attributed to stress increases in the surrounding areas induced by the rupture of the main shock [20]. However, although aftershocks and afterslips can partially release sudden stress increases in areas surrounding the main rupture, further study is still required concerning how and to what extent the stress state was changed there.

Pollitz et al. [21] and Ito et al. [22] have also recently characterized the Tohoku fault rupture based on the joint inversion of terrestrial GPS data and seafloor GPS/acoustic data. However, with slip maxima of 33 and 60 m, unexpected discrepancies were found between their results. Reasons for these discrepancies are not clear. With a linear fault rupture approximation, the fault plane of Pollitz et al. [21] is closer to the coastline, which will result in a smaller slip value. Furthermore, the study of Pollitz et al. [21] is similar to ours in the smoothing constraint applied in the inversion, whereas that of Ito et al. [22] did not use any smoothing constraint; this perhaps caused a larger slip value in their model.

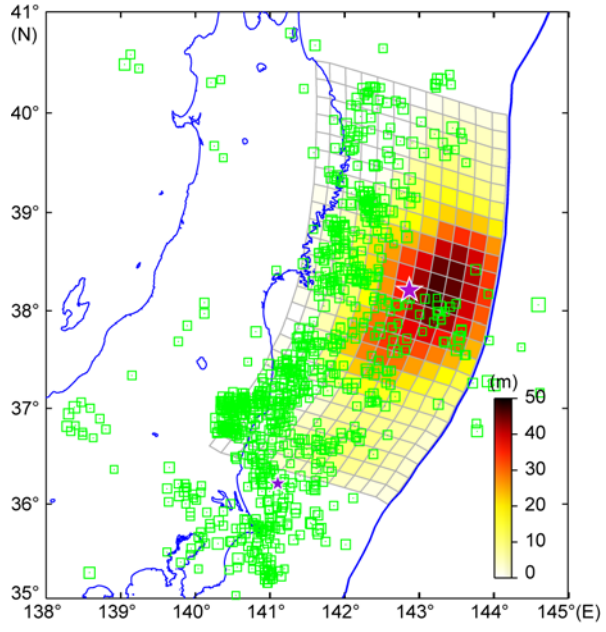

Figure 8 Spatial distribution of aftershocks and co-seismic slip distribution. The green square denotes aftershocks ($M > 4$) that occurred in the three months after the main shock (data from USGS).

4 Conclusions

Abundant geodetic observations, including terrestrial GPS data and seafloor GPS/acoustic data, provide an unprecedented chance for us to study the slip distribution of an M_w 9.0 earthquake. "Checkerboard" test shows that near-field seafloor GPS/acoustic data can significantly improve the resolution of slip on the fault, thereby providing a more reasonable slip model for this earthquake. With a curved fault surface and layered earth structure, our results illustrate that the "geodetic" moment magnitude of this earthquake is 9.01 and the maximum slip is ~ 45.8 m located at a depth of 13.5 km. Ruptures with slip exceeding 10 m mainly occur from 39.6 to 36.97°N, along almost 240 km of the trench. The area of concentrated slip mostly occurs at a depth shallower than 40 km, up-dip of the hypocenter.

We thank Dr. Wang Rongjiang of GFZ for providing the SDM inversion code. We are grateful to anonymous reviewers and the editor for their critical comments. This work was supported by the Knowledge Innovation Program of the Chinese Academy of Sciences (KZCX2-SW-142), the National Natural Science Foundation of China (41021003, 40974034 and 90814009) and the Key Project of Earthquake Science (201008007). The figures were made using open-source Generic Mapping Tools software [23].

1 Shao G, Li X, Ji C, et al. Focal mechanism and slip history of the 2011 M_w 9.1 off the Pacific coast of Tohoku Earthquake, constrained with teleseismic body and surface waves. Earth Planet Space, 2011, 63: 559–564
2 Ammon C J, Lay T, Kanamori H, et al. A rupture model of the 2011 off the Pacific coast of Tohoku Earthquake. Earth Planet Space, 2011, 63: 693–696
3 Lay T, Ammon C J, Kanamori H, et al. Possible large near-trench slip during the 2011 M_w 9.0 off the Pacific coast of Tohoku Earthquake. Earth Planet Space, 2011, 63: 687–692
4 Yoshida Y, Ueno H, Muto D, et al. Source process of the 2011 off the Pacific coast of Tohoku Earthquake with the combination of teleseismic and strong motion data. Earth Planet Space, 2011, 63: 565–569
5 Yoshida K, Miyakoshi K, Irikura K. Source process of the 2011 off the Pacific coast of Tohoku Earthquake inferred from waveform inversion with long-period strong-motion records. Earth Planet Space,

2011, 63: 577–582
6 Suzuki W, Aoi S, Sekiguchi H, et al. Rupture process of the 2011 Tohoku-Oki mega-thrust earthquake (*M* 9.0) inverted from strong-motion data. Geophys Res Lett, 2011, 38: L00G16
7 Yagi Y, Fukahata Y. Rupture process of the 2011 Tohoku-Oki earthquake and absolute elastic strain release. Geophys Res Lett, 2011, 38: L19307
8 Simons M, Minson S E, Sladen A, et al. The 2011 magnitude 9.0 Tohoku-Oki Earthquake: Mosaicking the megathrust from seconds to centuries. Science, 332: 1421–1425
9 Hao J L, Wang W M, Yao Z X. Source process of the 2011 M_w 9.0 Tohuko Japan earthquake. Sci China Earth Sci, 2011, 54: 1105–1109
10 Ozawa S, Nishinura T, Suito H, et al. Coseismic and postseismic slip of the 2011 magnitude-9 Tohoku-Oki earthquake. Nature, 2011, 475: 373–376
11 Diao F Q, Xiong X, Ni S D, et al. Slip model for the 2011 M_w 9.0 Sendai (Japan) earthquake and its M_w 7.9 aftershock derived from GPS data. Chin Sci Bull, 2011, 56: 1999–2005
12 Sato M T, Ishikawa N, Ujihara S, et al. Displacement above the hypocenter of the 2011 Tohoku-Oki earthquake. Science, 2011, 332: 1395
13 Miura S , Takahashi N, Nakanishi A, et al. Structural characteristics off Miyagi forearc region, the Japan Trench seismogenic zone, deduced from a wide-angle and refraction study. Tectonophysics, 2005, 407: 165–188
14 Huang Z, Zhao D, Wang L. Seismic heterogeneity and anisotropy of the honshu arc from the Japan trench to the Sea of Japan. Geophys J Int, 2011, 184: 1428–1444
15 Wang L, Wang R, Roth F, et al. After-slip and viscoelastic relaxation following the 1999 *M*7.4 Ízmit earthquake, from GPS measurements. Geophys J Int, 2009, 178: 1220–1237
16 Mooney W D, Laske G, Masters T G. CRUST 5.1: A global crustal model at 5°×5°. J Geophys Res, 1998, 103: 727–747
17 Hashimoto C, Noda A, Sagiya T, et al. Interplate seismogenic zones along the Kuril-Japan trench inferred from GPS data inversion. Nat Geosci, 2009, 2: 141–144
18 Loveless J P, Meade B J. Geodetic imaging of plate motions, slip rates, and partitioning of deformation in Japan. J Geophys Res, 2010, 115: B02410
19 Pollitz F F, Brooks B, Tong X, et al. Coseismic slip distribution of the February 27, 2010 M_w 8.8 Maule, Chile earthquake. Geophys Res Lett, 2011, 38: L09309
20 Mendoza C, Hartzell S H. Aftershock patterns and main shock faulting. Bull Seismol Soc Am, 1988, 78: 1438–1449
21 Pollitz F F, Bürgmann R, Banerjee P. Geodetic slip model of the 2011 *M*9.0 Tohoku earthquake. Geophys Res Lett, 2011, 38: L00G08
22 Ito T, Ozawa K, Watanabe T, et al. Slip distribution of the 2011 off the Pacific coast of Tohoku Earthquake inferred from geodetic data. Earth Planet Space, 2011, 63: 627–630
23 Wessel P, Smith W H F. Free software helps map and display data. Eos Trans Am Geoph, 1991, 72: 445–446